# Pattern formation in a rotating suspension of non-Brownian buoyant particles

Makrand G. Kalyankar,[1] W. R. Matson,[2] Penger Tong,[3] and Bruce J. Ackerson[1]
[1]*Department of Physics, Oklahoma State University, Stillwater, Oklahoma 74078, USA*
[2]*Department of Physics, DePaul University, 2219 North Kenmore Avenue, Chicago, Illinois 60614-3504, USA*
[3]*Department of Physics, Hong Kong University of Science and Technology, Clear Water Bay, Kowloon, Hong Kong*

(Received 1 April 2008; accepted 23 July 2008; published online 19 August 2008)

This study examines the concentration and velocity patterns observed in a horizontal rotating cylinder completely filled with a monodisperse suspension of non-Brownian buoyant particles. The unique patterns or phases are mapped by varying both the rotation rate and the solvent viscosity. Individual phases are identified using both frontal ($\theta$-$z$ plane) and axial ($r$-$\theta$ plane) views. Phase boundaries are compared to those obtained recently for suspensions of nonbuoyant particles. Expressing the boundaries in terms of dimensionless parameters unifies the data for several samples at low rotation rates. When centrifugal force dominates, the behavior becomes quite different from previous studies. © *2008 American Institute of Physics*. [DOI: 10.1063/1.2970156]

## I. INTRODUCTION

Particle laden flows have wide usage in industrial processes. Materials are transported by either gas (pneumatic transport) or liquids (slurry transport), depending on the specific application. Improved understanding of these flows[1–4] will have far reaching benefits in upgrading the operation and efficiency of current processes and in supporting the development of new and innovative processing techniques. In this experiment, we study the velocity and concentration patterns produced by suspensions of buoyant particles in a solvent that completely fills a horizontal rotating cylinder. There are a number of experiments examining the behavior of partially filled cylinders, where the suspension surface is essential to produce the observed concentration patterns.[5–11] Here there is no free surface producing patterns, yet a surprising number of velocity and concentration patterns have been observed.

Lipson and co-workers[12–14] discovered bands of high and low particle concentration spaced along the rotation axis of the cylinder. They measured the average band spacing $\lambda$ as a function of the cell length/radius ratio, $L/R$. Compared to our studies, the millimeter sized particles used in their experiment are quite large. The particle based Reynolds numbers, defined as $\mathrm{Re}_1 = 2aU_0\rho_f/\eta$, for their systems are correspondingly large being in the range between 6.5 and 735. Here $a$ is the particle radius, $U_0$ is the isolated particle settling velocity, $\rho_f$ is the solvent density, and $\eta$ is the solvent viscosity. Thus inertial effects[15,16] may well be important to the observed band pattern.

Breu *et al.*[17,18] studied suspensions of glass beads in a fully filled horizontal cylinder rotating at high speeds. They reported instability where the beads go from forming a layer on the inner wall of the rotating cylinder to forming radially symmetric rings upon lowering the rotation rate. This is similar to crossing the discontinuous banding (DB)/centrifugal limit (CL) phase boundary reported by Matson and co-workers.[19–21] Breu *et al.*[17,18] also observed particle traveling waves. Like Lipson *et al.*, the studies by Breu *et al.* occur at large Reynolds numbers ($\mathrm{Re}_1 \sim 20$).

The work by Matson and co-workers[19–21] occurs in systems with $\mathrm{Re}_1 < 0.1$. Hence inertia is not considered important. By varying the rotation rate $\omega$ and solvent viscosity $\eta$ over a wide range, Matson *et al.*[21] carefully studied the overall phase behavior of the rotating suspensions and mapped out the phase boundaries of some ten different patterns or phases. These systematic measurements have made it possible to find scaled representations of the phase boundaries that explain the same boundary in a variety of systems with different particle radii $a$, volume fractions $\phi$, and cylinder radii $R$.

Theoretical arguments and calculations[12–14,17,18,22,23] have been made to explain the observed flow patterns, but they made different assumptions and predictions. A generally accepted theoretical framework for the rotating suspension is yet to be obtained. Lee and Ladd[22] put forth a theory to explain axial segregation of suspension of settling particles observed by Matson *et al.*[19] They proposed that for particles denser than the surrounding fluid, differential centrifuging between particles at different radial positions leads to an attractive interaction. This attraction between pairs of particles produces a relative motion in the axial direction, independent of gravity, introducing rapid growth of axial density fluctuations. This mechanism was proposed as a cause of band formation in a rotating suspension of settling particles. Their theory also suggests that in a suspension of particles that are less dense than the suspending medium, any axial perturbation in concentration will decay due to stabilizing repulsive interactions. This result provided the initial impulse to do the work presented here. In a follow up paper, Lee and Ladd[23] reported the results of simulations to test their proposal. The Stokes flow simulation for patterns observed at low rotation rates by Matson *et al.*[19] revealed that the formation of axial

 

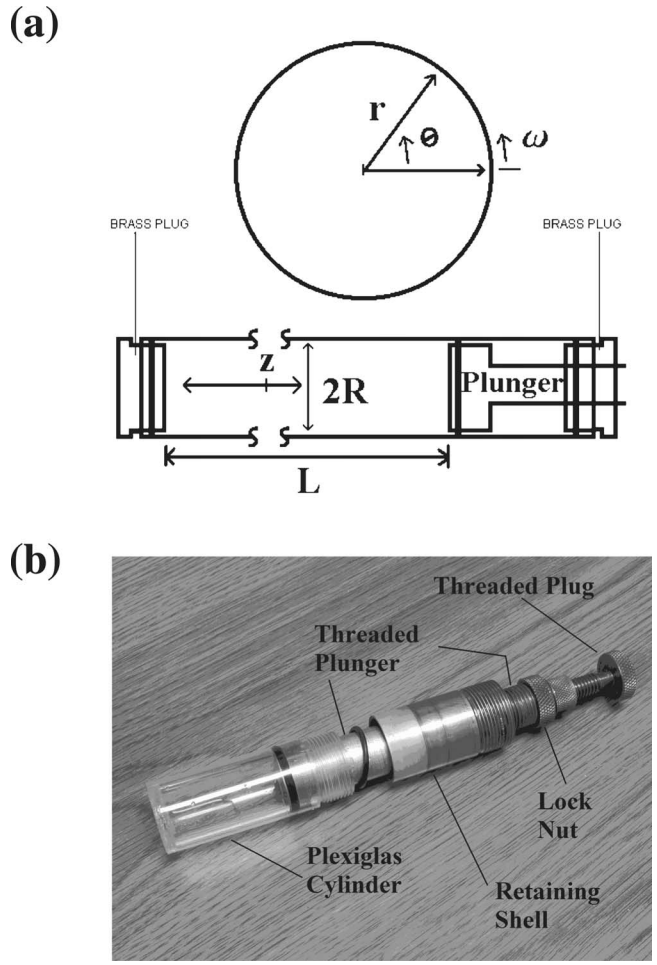


FIG. 1. (a) Construction of the long cylindrical sample cell (lower picture) and the cylindrical coordinates used to describe the measurements (upper picture). (b) Assembly of the short cell.

bands is correlated with an inhomogeneous particle distribution in the radial plane more than being driven by centrifugal forces.

Our current work examines the proposal of Lee and Ladd[22] experimentally. The use of buoyant particles allows us to change the sign of the density difference between the particle and fluid (solvent), $\Delta\rho \equiv \rho_p - \rho_f < 0$. As a result, the directions of the buoyancy force $\Delta\rho g$ and the centrifugal force $\Delta\rho\omega^2 R$ are changed. A comparative study of pattern forming dynamics in the buoyant and settling particle suspensions, therefore, will help us to identify the dominant forces involved in each of the steady state phases. It is found from the experiment that when gravity dominates centrifugal forces, the buoyant particle suspensions correlate with the settling particle suspensions. When centrifugal forces dominate, quite different phases appear, although they may still be related to the phases in settling particle suspensions.

## II. EXPERIMENTAL METHODS

The construction of the entire rotating cylinder system is the same as that used in our previous studies,[20] and here we mention only some key points. The lower picture in Fig. 1(a) shows the long cell used in the experiment. A Plexiglas cylinder with an internal diameter of 1.9 cm is mounted horizontally on a thermally isolated aluminum stand. The two brass ends are milled to seat *o*-rings, which seal the system when ends are inserted. One end has two *o*-rings and acts as a plunger for setting the effective length of the cell. In this experiment, the length is $L = 22.75 \pm 0.05$ cm. The other end has a threaded plug used to purge air from the cell. This cell rotates freely on two press fit ball bearing races.

The cell sits inside a rectangular Plexiglas chamber with a minimum clearance of 2.5 cm. Hydraulic *U*-cup seals allow the cell to rotate within the chamber with minimal leakage. A solution of water, glycerin, and soap is pumped through the chamber surrounding the rotating cylinder. Soap and glycerin prevent bubble formation on the surface of the rotating cylinder and increases visibility. The temperature of this solution is maintained at $\pm 0.05$ °C using a temperature control system (Thermo-Neslab Recirculator Bath). Precise control of the temperature of the circulating water eliminates any temperature gradient across the length of the tube. The precision of temperature control allows control of the sample viscosity to within 5%. The flat chamber surfaces improve optical illumination, imaging, and viewing of the sample by eliminating strong refraction of light at the cylindrical surface. The base plate of the aluminum stand has adjustable legs to ensure that the axis of rotation is horizontal.

A stepping motor drives the cell rotation. A microstepping controller triggered by a homemade indexer provides $2.5 \times 10^4$ steps/revolution with a rotation period ($T$) accuracy of $2.5 \times 10^{-2} \pm 2.5 \times 10^{-5}$ s. Thus the rotation rate ($\omega = 2\pi/T$) at a phase boundary can be determined with high accuracy. The motor drive is thermally isolated from the cell using a wooden linkage.

The upper picture in Fig. 1(a) shows the coordinate system used in this paper. Here $r$ and $\theta$ are the radial and azimuthal coordinates, with respect to the axis of rotation, respectively. The third dimension in this cylindrical coordinate system is $z$. In the experiment, we use a standard video imaging technique to record the motion and spatial distribution of the particles. A video charge-coupled device camera records particle images in different cross-sectional planes of the cylinder ($r$-$\theta$ plane) and in the $\theta$-$z$ plane (front view).

To make observations of the $r$-$\theta$ plane (end view), a second shorter cell with the same 1.9 cm internal diameter but with a transparent end window for video imaging is used. Figure 1(b) shows the assembly of the short cell. Again the cell length is adjustable and usually set to $L = 2.25 \pm 0.03$ cm, corresponding with the average length of a single "band" seen in one of the phases to be described. The length adjustment is achieved using a threaded plunger and a brass retaining shell. The short Plexiglas cylinder slides over the plunger until it contacts the brass retaining shell, where it is clamped tight using a setscrew. A lock ring is used on the threaded part of the plunger and on the back of brass shell to prevent vibration and rotational slippage of the brass shell and piston. The brass outer shell passes through a vertical support and is screwed into a thermal insulating shaft connected to motor drive. The vertical support houses a press fit ball bearing race and a *U*-cup seal to prevent friction and

leakage. A square Plexiglas thermal control chamber is anchored to the vertical support and completely encompasses the cell assembly. A laser light sheet of 1 mm in thickness illuminates the sample parallel to the $r$-$\theta$ plane. The vertical support may be moved in the $z$-direction to illuminate different portions of the 2.25 cm long cell. The motor drive is identical to that described above.

Buoyant particles prove significantly more difficult to load and purge of air than nonbuoyant particles that settle away from the air to be purged. Air bubbles have little influence on the phase formation. However, bubbles disturb local flow, causing streaks, and making phase identification difficult. Through trial and error, an efficient assembly and sample loading procedure was developed, which minimizes or eliminates air bubbles. Details about the assembly and loading are described in the Appendix.

An aqueous solution of glycerin is used as the medium for the experiment. The solution is prepared based on the range of viscosity desired. Our standard solution is 77 wt. % glycerin solution. A small amount (0.25 vol. %) of soap is added to the solution to prevent particles from aggregating. The viscosity of the solution varies from 19 to 100 cP when the temperature of the solution is changed from 44 to 6 °C.[24] Measurements of the solvent viscosity at different temperatures were conducted using a Bohlin rheometer, and the final result is well described by a polynomial within the experimental temperature range,[24]

$$\eta = 162.7 - 10.65x + 0.3193x^2 - (4.655 \times 10^{-3})x^3 + (2.654 \times 10^{-5})x^4, \quad (1)$$

where the viscosity $\eta$ is in units of cP and temperature $x$ is in units of °C. Any desired viscosity is selected by tuning the water bath to the appropriate temperature.

The suspended particles are hollow glass microspheres purchased from MO-SCI Corporation (Product No. GL-0237). According to the manufacturer, the density of the spheres is 0.15 $g/cm^3$ and particle's diameter ranges from 85 to 110 $\mu$m. We measure the particle size distribution from several calibrated particle images taken with a microscope. It is found that the particles have an average diameter of 96 $\mu$m with a standard deviation of 6 $\mu$m. The volume fraction of particles in the suspension is fixed at $\phi = 2.3\%$.

To study the phase behavior of the rotating suspension, the viscosity is scanned by increasing the temperature in increments of 5 °C over the entire temperature range. For each temperature setting, the cylinder is scanned through a range of rotation rates available, and the cell is monitored visually to identify steady state density and flow patterns. To determine phase boundaries, a phase is identified first and the rotation rate is changed by a reasonably large amount to bring the system into another phase. Then the rotation rate is returned by half the amount to the original value. The phase is identified and another step cutting the step size in half is made. This process continues until the desired accuracy is achieved.

## III. EXPERIMENTAL RESULTS

A particular "phase" corresponds to a region in the examined space of fluid viscosity and rotation period $\{\eta, T\}$ (or $\{\eta, \omega\}$) that has a characteristic concentration and/or velocity pattern. The structure in a "coexistence phase" changes continuously between bounding patterns. A phase boundary separates two objectively distinct phases in the phase space. There exists a specific sequence of phases through which the system progresses as the rotation rate $\omega$ increases. In this section, we first describe the general phase behavior of the buoyant suspension, followed by a discussion on how the transition boundaries change with the experimental control parameters.

### A. General phase behavior of the buoyant system

The buoyant particle suspension is chosen to closely match a settling particle suspension, whose phase diagram has been mapped out in a recent experiment.[21] The settling particle suspension was referred to as "small particle system" in Ref. 21. Hereafter, we refer to it as the "settling system." The buoyant particle suspension will be referred to as the "buoyant system." The relative density difference for the buoyant system is $\Delta\rho/\rho_f \simeq -0.87$, while for the settling system, it is $\Delta\rho/\rho_f \simeq 1.03$. The size of the hollow spheres is 96 $\mu$m, while for the settling system the particle diameter is 104 $\mu$m. Thus the hollow spheres drift upward at approximately the same rate as the solid spheres settle downward. Since experiments are done in identical cells, these two systems should correspond at least at low rotation rates.

The settling system exhibits a total of ten different steady states (or dynamic phases) and they are distinguished in the experiment by their unique flow patterns and particle distributions. At low rotation rates, the particles lie and slide at the bottom floor of the cylinder, forming a fluidized granular bed (GB). At very high rotation rates, the centrifugal force becomes dominant and all the particles are spun onto the cylinder wall. Between the two extremes, we observed a series of interesting concentration and velocity patterns in the rotating suspension. Figure 2 shows the "phase diagram" of the settling system as a function of the rotation period $2\pi/\omega$ and fluid viscosity $\eta$. It is reproduced here[21] to serve as a guide.

Now we describe the observed phases in the buoyant system in order of their appearance with increasing $\omega$. We compare and contrast these phases with those observed in the settling system. This discussion serves as an introduction to the buoyant system. Its phase behavior shares some common features with that of the settling system at high viscosities and low rotation rates where gravity dominates centrifugal forces. At lower viscosities and higher rotation rates, centrifugal forces become dominant and the two systems behave quite differently. Figure 3 shows the front view ($\theta$-$z$ plane) and Fig. 4 shows the end view ($r$-$\theta$ plane) of the observed phases in the buoyant system with increasing $\omega$. The front view images were taken usually using back lighting. Regions with higher particle population absorb and scatter more light and thus appear darker. Particle trajectories are visible as

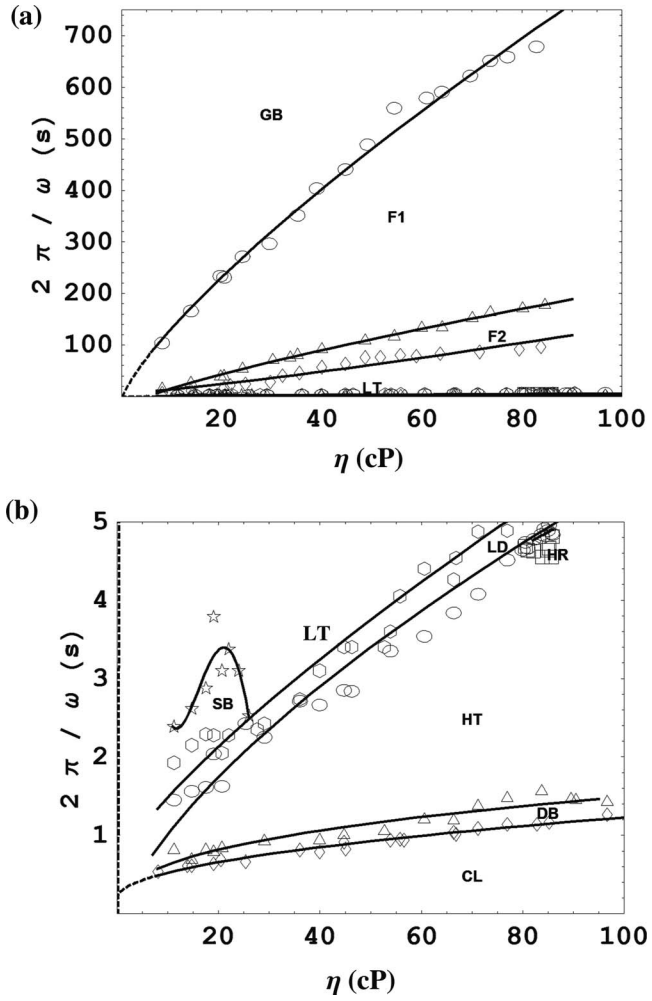


FIG. 2. (a) Overall phase diagram of the settling system in the plane of the rotation period $2\pi/\omega$ and fluid viscosity $\eta$. (b) An enlarged part of the phase diagram for high rotation rate states. The symbols are experimentally determined data points and the solid lines are spline-fitted smooth curves for the phase boundaries. The dashed lines are the extrapolated curves from the fit: GB, granular bed; F1, fingering flow I; F2, fingering flow II; LT, low-rotation-rate transition; SB, stable band; LD, local-structure dropout; HR, homogenous region; HT, high-rotation-rate transition; DB, discontinuous banding; and CL, centrifugal limit.

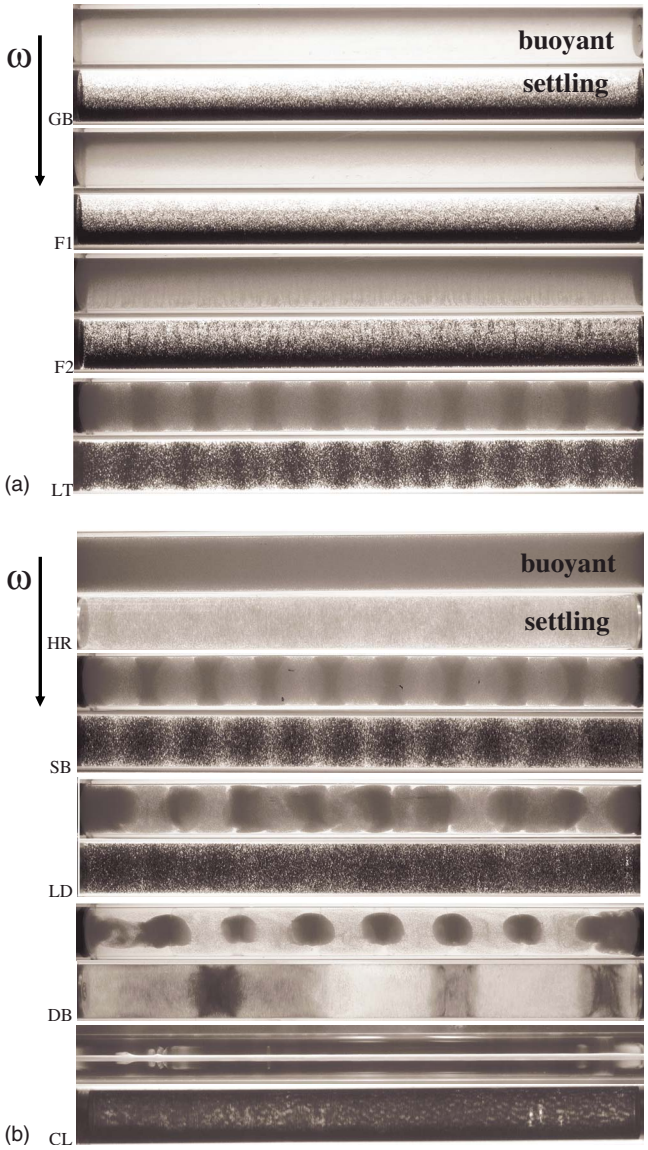


FIG. 3. (Color online) Front view ($\theta$-$z$ plane) of the observed phases in the buoyant system (upper images) with increasing $\omega$. The direction of increasing $\omega$ is marked by a long arrow. For comparison, the corresponding phase images for the settling suspension (lower images) are also included. All the front view images were taken using back lighting and darker regions have more particles; except the upper image of CL which was taken using front lighting with white color showing the particle concentrated region. From top to bottom the phases are (a) GB, F1, F2, and LT; (b) HR, SBs, LD, DB, and CL.

streaks in superposed consecutive images. For comparison, we also include the corresponding phase images for the settling suspension.

### *1. Granular bed*

In this phase, the particles accumulate at the top of the cylinder. As the cylinder rotates, the particles in the immediate vicinity of the cylinder wall are carried down with the falling wall of the cylinder. The particle buoyancy results in the innermost particles streaming upward along the surface of the GB. The streaming produces a circulation in the suspending fluid near the bed that is opposite the cylinder rotation. Hence, there are two types of fluid rotation inside the cylinder. The fluid near the GB moves clockwise due to buoyancy, while the bulk of the liquid is moving counterclockwise, being carried along with the cylinder. The clockwise rotating liquid pushes particles into the bed and stabilizes the bed. The inner layers of the bed evidence counterclockwise rotation with a small amount of disintegration. The flow inside the GB is complex but appears similar to a coating flow.[25]

Figure 4 (GB) compares the GB phase observed in the settling system with that observed in the buoyant system. The two phases are largely similar. The settling particles are dragged along the rising wall, whereas the buoyant particles are dragged along the falling wall. Because the effective direction of gravity is reversed between the two systems, rotation of either picture by 180° about the axis of rotation makes the patterns coincide.

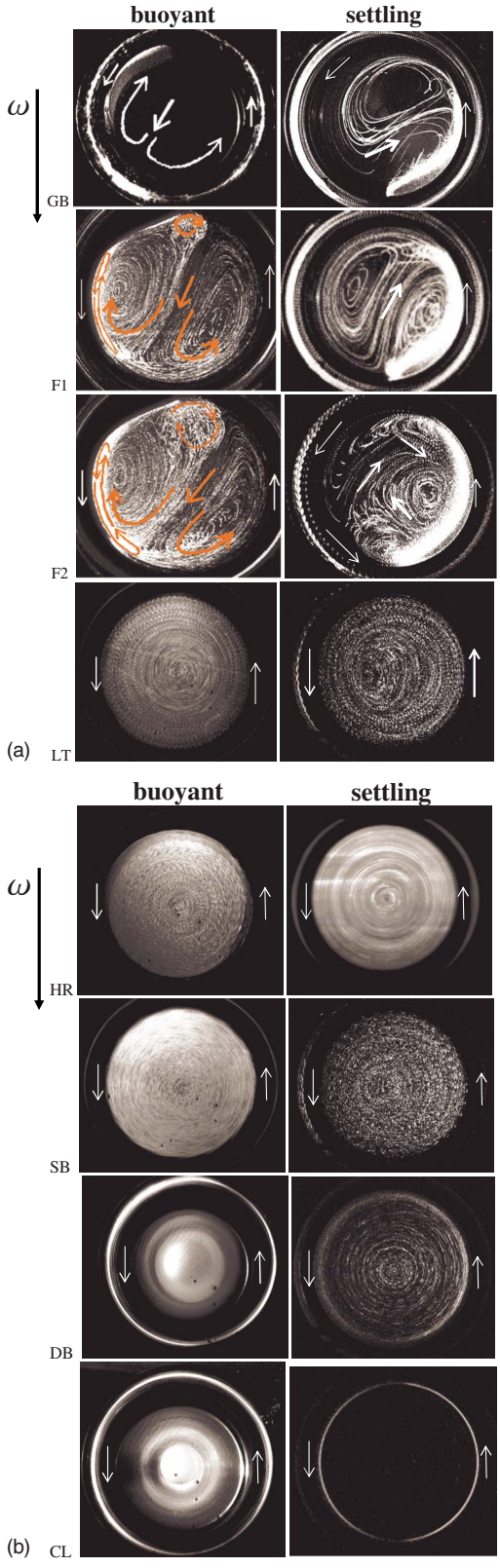


FIG. 4. (Color online) End view ($r$-$\theta$ plane) of the observed phases in the buoyant system (left images) with increasing $\omega$. The direction of increasing $\omega$ is marked by a long arrow. For comparison, the corresponding phase images for the settling suspension (right images) are also included. For clarity, 30 sequential images taken at time intervals ranged from 1 s (for low-$\omega$ states) to 1/30 s (for high-$\omega$ states) are superimposed and the contrast of the pictures is reversed with white streaks (particle trajectories) on a black background. The short arrows inside each image indicate the direction of the local flow and the cylinder rotation. From top to bottom the phases are (a) GB, F1, F2, and LT; (b) HR, SBs, DB, and CL.

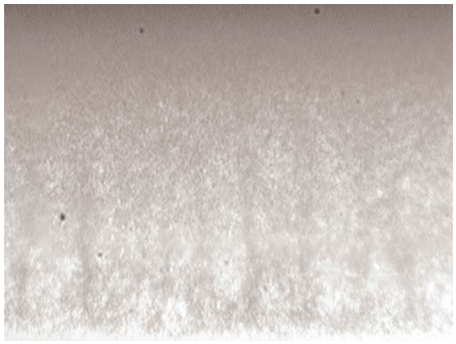

FIG. 5. (Color online) Closeup of front view ($\theta$-$z$ plane) of fingering. The dark streaks show the chainlike structures rise vertically in the direction of buoyancy forces. The displayed region is approximately 1.8 cm $\times$ 2.4 cm.

### 2. Fingering flow I

When the rotation rate is increased, the tail of the GB elongates. The effect of buoyancy increases as a particle descends lower. Once the particle crosses a critical angular displacement as the tube rotates, the buoyant force lifts the particle away from the wall, and the particle rises. As the particle makes its way through the liquid, it drags the neighboring particles in its wake. A chain of particles or a finger-like pattern emerges. This phenomenon is replicated along the entire length of the tube. From the front view it is clearly observed that at low rotation rates, the spacing between fingers is comparable to the finger width, only two to three particle diameter wide. At higher rotation rates (larger $\omega$), the spacing increases to several millimeters, while the fingers remain narrow by comparison. A closeup of fingering is shown in Fig. 5.

Fingers maintain their fixed radial distance from the rotation axis until they collide with the bed during their rise. As can be seen from the end view of the fingering flow I (F1) phase shown in Fig. 4 (F1), the flow divides the cylindrical cross section into two halves of counter-rotating flows. The narrow region, which divides the $r$-$\theta$ plane in half, behaves as a potential ridge keeping particles separated into one half or the other. Particles travel parallel to this ridge and do not cross the ridge. Any crossing of particles from one region to another happens near the trailing edge of the GB. A new circulation may be observed at the leading edge of the GB. This small circulation will eventually develop into a full-blown circulation giving rise to the next steady state phase.

The F1 phase exhibits similar physical manifestation to that described by Matson *et al.*[20] The buoyant system appears as the image of the settling system but rotated 180° about the rotation axis.

### 3. Fingering flow II

The small circulation at the leading edge of the GB becomes a full-blown circulation in this phase. This circulation divides the cross section of the tube into three parts. The tube now has two counter-rotating circulations and one corotating circulation. The remaining bed corotates as well. Particles in this new counter-rotating region exhibit closed orbits with different centers of rotation. The corotating circulation evolves into a pattern with shorter elongated orbits and oc-

cupies a smaller portion of the cross section of the cylinder. Analysis of the end view for this phase suggests that the particles constituting the fingers, as well as other suspended particles, always remain in the illuminating light sheet ($r$-$\theta$ plane). This suggests a two dimensional flow for this phase.

Comparative pictures shown in Fig. 4 [fingering flow II (F2)] reveal similarity of the settling and buoyant systems. Again the end views shown in Fig. 4 (F2) coincide if either is rotated by 180°. The counter-rotating circulation near the leading edge of the GB is more pronounced for the buoyant system.

#### 4. Low-rotation-rate transition

The low-rotation-rate transition (LT) phase is a coexistence phase. The phase represents the onset of secondary flows with components parallel to the axis of rotation. The flow structure of this phase evolves continuously from the F2 flow to the band formation. Compared to the stable band (SB) phase, however, the bands observed in the LT phase, as shown in Fig. 3 (LT), are not stable and are not isolated from one another. Figure 4 (LT) shows complete destruction of the GB. It also shows the beginning of corotation of all particles with the cell. The bandlike structures seen in Fig. 3 (LT) are not isolated from one another and share particles. The effect of nonzero velocity parallel to the axis of rotation can be correlated with the unstable center of rotation seen in Fig. 4 (LT). The buoyant and settling systems are mostly identical for the LT phase.

#### 5. Homogeneous region

This phase occurs for only a small range of viscosity and rotation rate space. All secondary flows become negligible, leaving a nearly uniform concentration across the entire cylinder with the suspension in nearly rigid rotation with particle velocity approximately $r\omega$. Uniform concentration throughout the tube is evident in the pictures shown in Fig. 3 [homogeneous region (HR)]. It is interesting to note that for the buoyant system this phase occurs between the LT and SB phases. For the settling system, however, this phase occurs between the local-structure dropout (LD) and high-rotation-rate transition (HT) phases.

#### 6. Stable bands

The evolution to the SB phase from the LT is characterized by the formation of SBs, where the bands remain fixed in position and isolated from one another. To be categorized as the SB, bands must be structurally indistinguishable, symmetric about their maximum concentration line, time independent in behavior, and isolated from their neighbors. Bands do not share particles. The line of maximum concentration is vertical and stationary. The velocity field within a single band runs parallel to the particle rich-particle poor boundary and is symmetric about the line of maximum concentration. The band structure is identical for both the settling and buoyant systems, as seen in the comparative pictures in Fig. 3 (SB). In an early experiment, Lipson[26] reported that small air bubbles trapped inside a rotating fluid also form band structures.

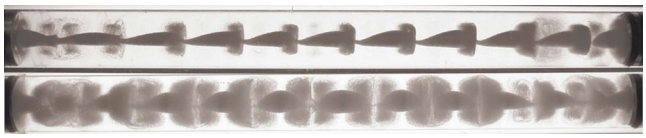

FIG. 6. (Color online) Cone structure formation in the DB phase at two slightly different rotation rates near the CL boundary. The lower picture is further from the CL transition. Darker regions have more particles.

#### 7. Local-structure dropout

LD is the first phase that evidences differences from the settling system. In the case of the settling particle phase, redistribution of the particles because of the LD begins at one location and then spreads from that location along the $z$-axis in both directions as the rotation rate increases. For buoyant particles, the SB structure disintegrates as all the bands become unstable simultaneously with increasing $\omega$. They oscillate, lose symmetry, and are not isolated from one another. The system enters into a mode exhibiting spatiotemporal chaos, where particles continuously exchange between the unstable structures shown in Fig. 3 (LD). Observations over couple of days failed to evidence any sort of steady state phase with a definite stable pattern.

#### 8. Discontinuous banding

At higher rotation rates, the chaotic mode of the system is replaced by axial concentration discontinuities, where the particle concentration comes to an abrupt halt (or start). This phase is the analog of the segregation bands described in Ref. 20. Segregation bands collectively contain the entire particle population of the cylinder. Particles near the cylinder wall are swept into these bands. For the DB phase studied here, the particles in these bands tend to collapse toward the axis of the cylinder, as shown in Fig. 3 (DB) and Fig. 4 (DB). The structure of the isolated bands is similar to the structure of single band in the SB phase. The band is wider near the descending wall than the ascending wall. It has the appearance of a 60° section cut from a doughnut. Individual particle orbits lie in the vertical planes. It is unclear whether a hole on the rotation axis passes completely through this structure. A small fraction of particles is ejected out from the center of the hole. At the higher rotation rate boundary of this phase, before transforming into centrifugal limit (CL), the phase morphs its axial discontinuities to a tenuously connected chain of conelike structures, as shown in Fig. 6. Note the asymmetry of these structures with respect to the axis of rotation.

#### 9. Centrifugal limit

The highest rotation rate phase is dominated by the centrifugal force. For the settling system, this phase results in a uniform coating of particles on the inner cylinder wall. On the other hand, for the buoyant system, this phase results in all the particles collapsing into a uniform cylinder centered on the axis of rotation, as shown in Fig. 3 (CL). Based on a measurement of the radius of this cylinder and the volume fraction of particles in the sample, we estimate a volume fraction of 0.62 for the particles contained in the cylindrical

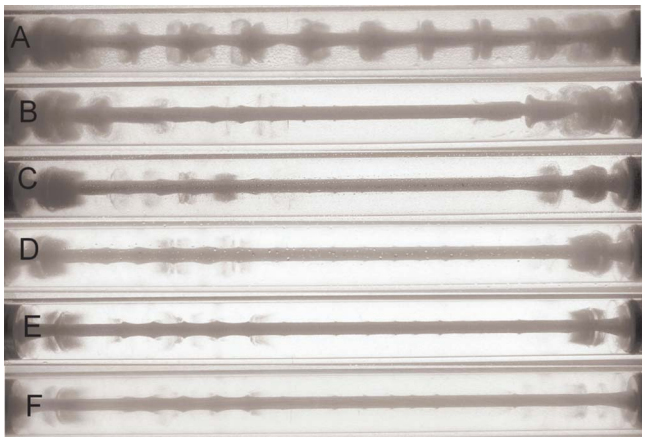


FIG. 7. (Color online) Transition of the DB phase (a) into the CL phase [(a)–(f)] when a 0.025 s change in rotation period is made.

structure. This is nearly the value of 0.6328 determined for the random close packing of hard spheres.[27] The onset of this phase is one of the sharpest transitions, as it is for the settling system. Figure 7(a) shows the last stable state in the DB phase. Decreasing the rotation period by 0.025 s, the limit of resolution of our apparatus, leads to a quick collapse into the CL phase. This collapse is documented in the remaining pictures in Figs. 7(b)–7(f).

In summary, the behavior of the buoyant system corresponds with the settling system at high viscosities and lower rotation rates, when accounting for the direction of movement with respect to gravity. The physical manifestation of the phases at lower viscosities and higher rotation rates is very different for buoyant particles as compared to settling particles. There exists a specific sequence of phases through which both systems progress as $\omega$ increases. The sequence and the phases observed are not identical for both systems. The HR phase observed before onset of the HT phase for the settling system is observed before the SB phase for the buoyant system. Also, contrary to the settling system, which exhibits a set of ten different steady states, the buoyant system shows only nine different steady states. Conspicuously absent is the HT phase.

### B. Scaling properties of the transition boundaries

Transition boundaries for the buoyant system are determined for the GB/F1, F1/F2, F2/LT, and DB/CL phases and compared to the corresponding phase boundaries for the settling systems with the relative density difference $\Delta\rho/\rho_f \simeq 1.03$. The phase boundaries for all our settling systems with different particle radii, volume fractions, and cylinder radii have been expressed in dimensionless units to find a single expression for each boundary.[21] It was found that in the low rotation rate regime (regime I), which includes the GB, F1, F2, and part of LT phases, hydrodynamic interactions resulting from the settling of individual particles are important. The transition boundaries in this regime can all be described by three dimensionless parameters: $a/R$ (the ratio of the particle radius $a$ to the cylinder radius $R$), $1/\mathrm{Re}_3 \equiv \eta/(\rho_f \omega R^2)$ (the ratio of the viscous force to the centrifugal force), and $A \equiv \Delta\rho g/(\rho_f \omega^2 R)$ (the ratio of the buoyancy force to the centrifugal force). The phase boundaries of the buoyant system are similarly reduced and added to the existing data.

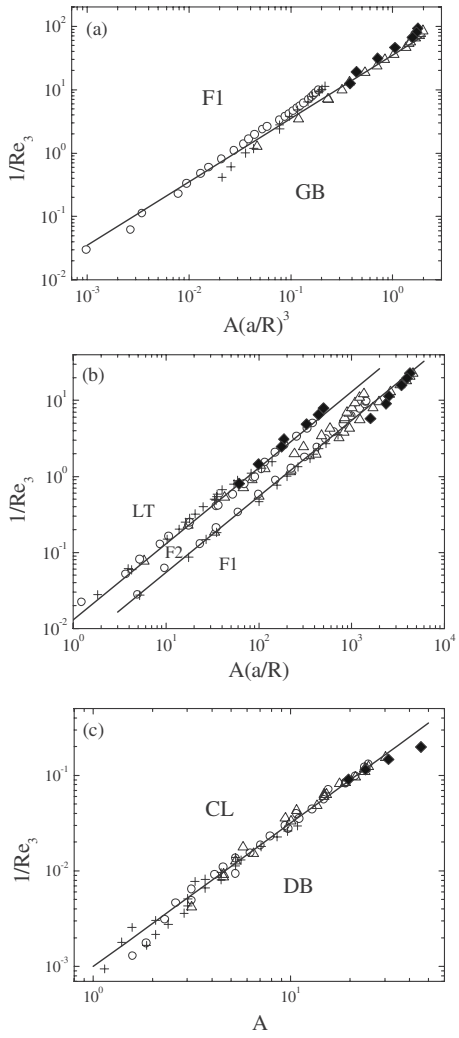


FIG. 8. Comparison of the scaled transition boundaries. Circles, triangles, and pluses are obtained, respectively, in the settling systems with (i) particle radius $a=100$ $\mu$m and cylinder radius $R=0.955$ cm (circles), (ii) $a=52$ $\mu$m and $R=0.955$ cm (triangles), and (iii) $a=100$ $\mu$m and $R=1.85$ cm (pluses). Solid diamonds show the buoyant system. (a) Transition boundary GB/F1 in the plane of $1/\mathrm{Re}_3$ and $A(a/R)^3$. The solid line is a power-law fit $1/\mathrm{Re}_3=35A(a/R)^3$. (b) Transition boundaries F1/F2 (lower curve) and F2/LT (upper curve) in the plane of $1/\mathrm{Re}_3$ and $A(a/R)$. The solid lines are the power-law fits $1/\mathrm{Re}_3=5.5\times10^{-3}A(a/R)$ (lower solid line) and $1/\mathrm{Re}_3=1.3\times10^{-2}A(a/R)$ (upper solid line). (c) Transition boundary DB/CL in the plane of $1/\mathrm{Re}_3$ and $A$. The solid line is a power-law fit $1/\mathrm{Re}_3=1.0\times10^{-3}A^{1.5}$.

Figure 8 shows log-log plots of four different transition boundaries. The GB/F1 boundaries obtained in both the settling and buoyant systems collapse nicely into a single master curve when they are plotted in the plane of $1/\mathrm{Re}_3$ and $A(a/R)^3$, which are two dimensionless variables for the experimental variables of $\eta$ and $\omega$. Curved boundaries in the linear plots shown in Fig. 2 become a universal straight line, as shown in Fig. 8(a), indicating that the GB/F1 boundary can be described by a power law, $1/\mathrm{Re}_3=\alpha[A(a/R)^3]^\beta$, with $\alpha=35$ and $\beta=1.0$ (solid line). The F1/F2 and F2/LT bound-

TABLE I. Numerical values of the measured transition boundaries of the buoyant system in the plane of $2\pi/\omega$ and $\eta$.

| GB/F1 | | F1/F2 | | F2/LT | | DB/CL | |
|---|---|---|---|---|---|---|---|
| $\eta$ (cP) | $2\pi/\omega$ (s) | $\eta$ (cP) | $2\pi/\omega$ (s) | $\eta$ (cP) | $2\pi/\omega$ (s) | $\eta$ (cP) | $2\pi/\omega$ (s) |
| 85 | 713.13 | 85 | 176.875 | 85 | 60.625 | 100 | 0.29 |
| 75 | 703.74 | 75 | 171.125 | 75 | 56.875 | 90 | 0.24 |
| 65 | 671.86 | 65 | 159.375 | 65 | 49.00 | 80 | 0.21 |
| 55 | 551.25 | 55 | 136.25 | 55 | 37.00 | 70 | 0.19 |
| 45 | 453.75 | 45 | 131.875 | 45 | 36.00 | | |
| 35 | 356.25 | 35 | 108.75 | 35 | 27.125 | | |
| 25 | 331.25 | | | 25 | 21.25 | | |

aries obtained in the settling and buoyant systems can also be brought into coincidence once they are plotted in the $1/\mathrm{Re}_3$ and $A(a/R)$ planes. This is shown in Fig. 8(b). The two boundaries can be described by a common power law, $1/\mathrm{Re}_3=\alpha[A(a/R)]^{\beta}$, with $\alpha=5.5\times10^{-3}$ and $\beta=1.0$ for the F1/F2 boundary (lower solid line) and $\alpha=1.3\times10^{-2}$ and $\beta=1.0$ for the F2/LT boundary (upper solid line). From Figs. 8(a) and 8(b), we find that the transition boundaries in regime I can be described by a simple condition, $C=U_0/(\omega a)=(U_0/\omega R)(R/a)=(2/9)A\ \mathrm{Re}_3(a/R)$, where $U_0$ is the settling (rising) velocity of the particles. In the above, $C$ is a constant for the F1/F2 and F2/LT boundaries, while it is dependent on $R/a$ for the GB/F1 boundary. The first equality, $U_0/(\omega a)$, shows no dependence on $R$, while the following equalities show the dependence on the velocity ratio $U_0/(\omega R)$, where $\omega R$ is the wall speed, and on the force ratios $A$ and $\mathrm{Re}_3$.

Figure 8(c) shows a log-log plot of the DB/CL boundaries in the plane of $1/\mathrm{Re}_3$ and $A$. The DB/CL boundaries in both the settling and buoyant systems collapse into a single master curve when they are plotted in the plane of $1/\mathrm{Re}_3$ and $A$. Curved boundaries in the linear plots shown in Fig. 2 become a universal straight line, indicating that the DB/CL boundary can be described by a power law, $1/\mathrm{Re}_3\simeq\alpha A^{\beta}$ with $\alpha=1.0\times10^{-3}$ and $\beta=1.5$ (solid line). The transition boundaries in the high rotation rate regime have been shown to be independent of the particle size;[21] thus, we expect $\mathrm{Re}_3$, $A$ and $\phi$ to be the only important dimensionless parameters in this regime. The DB/CL boundary in the buoyant system has been scaled by a factor of 4.5 to compare with the corresponding boundary in the settling systems. Namely, the diamonds shown in Fig. 8(c) are obtained using a newly defined effective rotation period, $T'\equiv2\pi/\omega'=4.5(2\pi/\omega)$. Because the centrifugal force depends on both the rotation rate and the radial position in the cell, a larger rotation rate is required to hold buoyant particles near the center of the cell than settling particles on the cell wall. The fitting factor 4.5 accounts for this change in force. As a rough estimate, we equate the centrifugal forces required for the two systems and find that the resulting rotation rate $\omega_b$ for the buoyant particles is given by $\omega_b=(\Delta\rho_s/\Delta\rho_b)^{1/2}(R/r)^{1/2}\omega_s\simeq2.9\omega_s$, where $\omega_s$ is the corresponding rotation rate for the settling particles and $r$ is the radius of the buoyant particle rod formed on the axis of rotation, as shown in Fig. 3 (CL). The estimated number is close to but somewhat smaller than the fitted value, indicating that the centrifugal force may have different effects on the two systems.

It should be noted that the log-log plots in Fig. 8 are chosen to show the simple power laws discussed above. We recognize that these power laws are empirical and one may want to plot the data in different ways. To accommodate such needs, we provide the numerical values of the measured transition boundaries of the buoyant system in Table I.

## IV. CONCLUSION

This study extends the earlier work of Matson and co-workers[19–21] to include suspensions having buoyant particles. For gravitationally dominated flows, the buoyant and settling particle suspensions prove identical, when accounting for the effect of gravity on the particles. On the other hand, for centrifugally dominated flows, differences arise because the particles respond differently with respect to where they accumulate in the cell. Both the buoyant and settling systems produce a large array of phases that are identical or have similar properties.

The differential centrifuging theory of Lee and Ladd[22] is not supported experimentally, as the buoyant and settling systems both produce a SB phase. This theory predicted that settling particles experience an effective attraction leading to band formation, while buoyant particles experience an effective repulsion that disperse inhomogeneities in particle concentration. Of course, differential acceleration between particles and solvent is required because neutrally buoyant particles produce no SB or other phases in the absence of a free surface.[7] The two systems evidence a difference in the order of the appearance of the phases. The HR phase is observed between LT and SB phases for the buoyant system, whereas it is observed between LD and HT phases for the settling system. We have no explanation for the difference but expect it to be related to the centrifugal force.

Pattern selection by the rotating suspension is found to be independent of initial conditions; no hysteresis was observed contrary to the observations of Breu *et al.*[18] Cylinder length influences the number of periodic structures developed but does not affect the transition boundaries. The

DB/CL transition is very sharp in terms of the rotation rate. The conelike structures that occur just below the CL phase are the most unexpected structures observed in this study. As shown in Fig. 6, this structure has a strange symmetry property with respect to the axis of rotation. The narrowest part of the cone appears to align with the axis of rotation. This is the organization of the CL phase. On other hand, the wider portions of the cone appear to rotate around an axis off-set from the axis of rotation, similar to the axis off-set orbits of isolated particles.[28]

## ACKNOWLEDGMENTS

P.T. acknowledges support from the Research Grants Council of Hong Kong SAR under Grant No. HKUST-CA05/06.SC01.

## APPENDIX: ASSEMBLY AND SAMPLE LOADING PROCEDURE

The assembly and loading of buoyant particles should be done in the following order:

(1) Assemble the cell with the $z$-axis vertical initially.
(2) Insert the threaded brass end into the Plexiglas cylinder.
(3) Press fit this end into the ball bearing race mounted on the support stand.
(4) Load the cylinder with the desired solution.
(5) Siphon off any air bubbles (be sure that there are no air bubbles on surfaces inside the cylinder).
(6) Insert the adjustable brass plunger to the desired length (22.75 cm).
(7) Force any air bubbles out through the opening in the plunger (the tube now should be completely purged of air).
(8) Insert the assembly into the water jacket.
(9) Insert from the open side of the water jacket and press fit into the Plexiglas cell the brass plug which slides over the adjustable plunger.
(10) Fill the hollow portion of the plunger with solution.
(11) Place the assembly on a 2° incline, so the solution does not drain out through the open end of the plunger.
(12) Connect the entire assembly to the constant temperature bath.
(13) Rotate the cell at high rotation rate without inserting the end screw. Centrifugal force will trap any bubbles, if present, at the axis of rotation. These bubbles will rise along the axis of rotation and escape through the hole in the plunger.
(14) Inject particles through the orifice in the adjustable plunger using a syringe fitted with a long flexible tube. The preparation of the syringe is time consuming and must be done with great care. The goal is to eliminate all air and produce a well-mixed suspension of beads in the glycerin and water solution. If air is inserted during this process, air bubbles are produced and are very difficult to remove. Since the beads float, it is impractical to wash them as done in the case of the settling system discussed in Ref. 24 to remove trapped air between particles. The trick is to wash the beads in the syringe itself. The syringe is filled halfway and the beads are then introduced. Then the syringe is filled to the brim. The beads will rise to the surface, with bubbles of air trapped between them. These air bubbles are sucked out using a pipette. This process is repeated until no air bubbles remain. The syringe plunger is put in place and the syringe is place upside down so that the beads rise to the injecting end. The beads are then injected in the tube. Excess fluid will drain out.
(15) Press fit the support mount on the unmounted end.
(16) Put the end screw in place to seal the system.
(17) Mount the assembly on the base plate and connect the motor with the thermal insulating linkage.
(18) Use the leveling screws to make the axis of rotation horizontal. A rough leveling is performed using a liquid level indicator. Further leveling adjustments are made by slowly rotating the cell so that the beads form a line at the top of the tube. Precise leveling is achieved when the particles become distributed uniformly along the tube.

[1] M. C. Roco, *Particulate Two-Phase Flow* (Butterworth-Heinemann, Boston, 1996).
[2] U. Schaflinger, *Flow of Particles in Suspensions* (Springer-Verlag, Wien, 1996).
[3] C. Crowe, M. Sommerfeld, and Y. Tsujiet, *Multiphase Flows with Droplets and Particles* (CRC, Boca Raton, 1998).
[4] C. Voltz, W. Pesch, and I. Rehberg, "Rayleigh–Taylor instability in a sedimenting suspension," Phys. Rev. E **65**, 011404 (2001).
[5] O. A. M. Boote and P. J. Thomas, "Effects of granular additives on transition boundaries between flow states of rimming flows," Phys. Fluids **11**, 2020 (1999).
[6] P. J. Thomas, G. D. Riddell, S. Kooner, and G. P. King, "Fine structure of granular banding in two-phase rimming flow," Phys. Fluids **13**, 2720 (2001).
[7] M. Tirumkudulu, A. Tripathi, and A. Acrivos, "Particle segregation in monodisperse sheared suspensions," Phys. Fluids **11**, 507 (1999).
[8] M. Tirumkudulu, A. Mileo, and A. Acrivos, "Particle segregation in monodisperse sheared suspensions in a partially filled rotating horizontal cylinder," Phys. Fluids **12**, 1615 (2000).
[9] B. D. Timberlake and J. F. Morris, "Concentration band dynamics in free-surface Couette flow of a suspension," Phys. Fluids **14**, 1580 (2002).
[10] N. P. Duong, A. E. Hosoi, and T. Shinbrot, "Periodic knolls and valleys: Coexistence of solid and liquid states in granular suspensions," Phys. Rev. Lett. **92**, 224502 (2004).
[11] P. Raiskinmaki, J. A. Astrom, M. Kataja, M. Latva-Kokko, A. Koponen, A. Jasberg, A. Shakib-Manesh, and J. Timonen, "Clustering and viscosity in a shear flow of a particulate suspension," Phys. Rev. E **68**, 061403 (2003).
[12] S. G. Lipson and G. Seiden, "Particle banding in rotating fluids: A new pattern-forming system," Physica A **314**, 272 (2002).
[13] G. Seiden, S. G. Lipson, and J. Franklin, "Oscillatory axial banding of particles suspended in a rotating fluid," Phys. Rev. E **69**, 015301(R) (2004).
[14] G. Seiden, M. Ungarish, and S. G. Lipson, "Banding of suspended particles in a rotating fluid-filled horizontal cylinder," Phys. Rev. E **72**, 021407 (2005).
[15] J. Happel and H. Brenner, *Low Reynolds Number Hydrodynamics*, 2nd ed. (Noordhoff, Leiden, 1973).
[16] H. K. Tsao and D. L. Koch, "Simple shear flows of dilute gas-solid suspensions," J. Fluid Mech. **296**, 211 (1995).
[17] A. P. J. Breu, C. A. Kruelle, and I. Rehberg, "Pattern formation in a rotating aqueous suspension," Europhys. Lett. **62**, 491 (2003).
[18] A. P. J. Breu, C. A. Kruelle, and I. Rehberg, "Oscillatory patterns in a rotating aqueous suspension," Eur. Phys. J. E **13**, 189 (2004).
[19] W. R. Matson, B. J. Ackerson, and P. Tong, "Pattern formation in a rotating suspension of non-Brownian settling particles," Phys. Rev. E **67**, 050301(R) (2003).

[20]W. R. Matson, M. Kalyankar, B. J. Ackerson, and P. Tong, "Concentration and velocity patterns in a horizontal rotating suspension of non-Brownian settling particles," Phys. Rev. E **71**, 031401 (2005).
[21]W. R. Matson, B. J. Ackerson, and P. Tong, "Measured scaling properties of the transition boundaries in a rotating suspension of non-Brownian settling particles," J. Fluid Mech. **597**, 233 (2008).
[22]J. Lee and J. C. Ladd, "Axial segregation in a cylindrical centrifuge," Phys. Rev. Lett. **89**, 104301 (2002).
[23]J. Lee and J. C. Ladd, "Axial segregation of a settling suspension in a rotating cylinder," Phys. Rev. Lett. **95**, 048001 (2005).
[24]W. R. Matson, "Pattern formation in a rotating suspension of non-Brownian settling particles," Ph.D. thesis, Oklahoma State University, 2004; also available at http://physics.ust.hk/penger/Matson.pdf.
[25]S. T. Thoroddsen and L. Mahadevan, "Experimental study of coating flows in a partially-filled horizontally rotating cylinder," Exp. Fluids **23**, 1 (1997).
[26]S. G. Lipson, "Periodic banding in crystallization from rotating supersaturated solutions," J. Phys.: Condens. Matter **13**, 5001 (2001).
[27]J. D. Bernal and J. L. Finney, "Random close-packed hard-sphere model," Discuss. Faraday Soc. **43**, 60 (1967).
[28]G. O. Roberts, D. M. Kornfeld, and W. W. Fowlis, "Particle orbits in a rotating liquid," J. Fluid Mech. **229**, 555 (1991).